

On Precision of the Leptonic Mixing Angle θ_{23} and its Implications for the Flavor Models

P. T. Quyen^{1,2,*}, S. Cao^{1,*}, N. T. Hong Van³, Ankur Nath⁴, and T. V. Ngoc⁵

¹*Institute for Interdisciplinary Research in Science and Education, ICISE, Quy Nhon, Vietnam.*

²*Graduate University of Science and Technology, Vietnam Academy of Science and Technology, Hanoi, Vietnam.*

³*Institute of Physics, Vietnam Academy of Science and Technology, Hanoi, Vietnam.*

⁴*Department of Physics, Namrup College, Assam, India*

⁵*Department of Physics, Kyoto University, Kyoto, Japan*

(Dated: October 29, 2024)

Among three leptonic mixing angles, θ_{23} angle, which characterizes the fractional contribution of two flavor eigenstates ν_μ and ν_τ to the third mass eigenstate ν_3 , is known to be the largest but the least precisely measured. The work investigates possible reach of θ_{23} precision with two forthcoming gigantic accelerator-based long-baseline neutrino experiments, namely Hyper-Kamiokande (T2HK) and DUNE experiments as well as a possible joint analyses of future neutrino facilities. Our simulation yields that each experiment will definitely establish the octant of θ_{23} angle for all values within 1σ parameter interval, while considering the current limitation. However, if the actual value is $0.48 \leq \sin^2 \theta_{23} \leq 0.54$, it becomes challenging for these two experiments to reject the maximal ($\theta_{23} = \pi/4$) hypothesis and conclude its octant. This octant-blind region can be further explored with the proposed facilities ESSnuSB and a neutrino factory. Accurate determination of the mixing angle θ_{23} , as well as the accuracy of δ_{CP} , is crucial for examining a certain category of discrete non-Abelian leptonic flavor models. Specifically if CP is conserved in leptonic sector, the combined analysis of T2HK and DUNE will rule out the majority of these models. However, if the CP is maximally violated, higher precision of δ_{CP} is necessary for testing these flavor models.

I. CURRENT UNDERSTANDINGS OF NEUTRINO OSCILLATION PARAMETERS

Observation of neutrino oscillation phenomenon [1–3] revolutionizes particle physics at the dawn of the twenty-first century since its implications of massive neutrinos and leptonic mixing are not adequately explained by the Standard Model of elementary particles. The up-to-date data [4], with few anomaly exceptions, can be well-described by a three-flavor neutrino model based on a 3×3 unitary mixing matrix known as Pontecorvo–Maki–Nakagawa–Sakata (PMNS) matrix [5, 6]. The matrix represents the magnitude of the coupling between three neutrino mass eigenstates (ν_1, ν_2, ν_3) and three charged-lepton states (e, μ, τ). The PMNS matrix is conventionally parameterized by three mixing angles ($\theta_{12}, \theta_{13}, \theta_{23}$), one Dirac CP-violation phase δ_{CP} , and additional two Majorana CP-violation phases if the neutrinos are Majorana particles. Measurements using neutrino oscillation phenomena, which are not affected by the Majorana phases, enable us to determine the four PMNS oscillation parameters ($\theta_{12}, \theta_{13}, \theta_{23}, \delta_{CP}$) and the neutrino mass-squared splittings, represented as $\Delta m_{ij}^2 = m_i^2 - m_j^2$ where $(i, j) = 1, 2, 3$. The neutrino

oscillation measurements typically involve two types of data samples: (i) the survival or *disappearance* of an α -flavor from the neutrino production source, and (ii) the *appearance* of a β -flavor from the α -flavor neutrino production source. The aforementioned process is observed in the survivals of ν_e from sun, $\bar{\nu}_e$ from the reactors and $\nu_\mu(\bar{\nu}_\mu)$ from the atmospheric and from accelerator-based sources. The *appearances* of $\nu_e(\bar{\nu}_e)$ and $\nu_\tau(\bar{\nu}_\tau)$ from atmospheric and accelerator-based sources of $\nu_\mu(\bar{\nu}_\mu)$ exemplify the later process. The probability of α -flavor neutrinos with energy E transitioning into β -flavor neutrinos observed at a distance of L in vacuum can be expressed as

$$P(\nu_\alpha \rightarrow \nu_\beta) = \delta_{\alpha\beta} - 4 \sum_{i>j} \Re(U_{\alpha i}^* U_{\beta i} U_{\alpha j} U_{\beta j}^*) \sin^2 \Phi_{ij} \pm 2 \sum_{i>j} \Im(U_{\alpha i}^* U_{\beta i} U_{\alpha j} U_{\beta j}^*) \sin 2\Phi_{ij}$$

where $\Phi_{ij} = \Delta m_{ij}^2 \frac{L}{4E} \equiv 1.27 \times \Delta m_{ij}^2 [\text{eV}^2] \frac{L[\text{km}]}{E[\text{GeV}]}$ and \pm sign is taken for neutrinos and anti-neutrinos, respectively. There are two well-established scales for neutrino mass-squared splittings: $\Delta m_{21}^2 \sim 7.4 \times 10^{-5} \text{ eV}^2/c^4$ and $|\Delta m_{31}^2| \sim 2.5 \times 10^{-3} \text{ eV}^2/c^4$. A crucial point to emphasize is that the positive or negative nature of Δm_{31}^2 remains unknown at yet. Therefore, it is currently unknown whether neutrino mass spectrum adheres to the *normal* ordering ($m_3 > m_2 > m_1$) or *inverted* ordering ($m_2 > m_1 > m_3$). Experiments T2K [7], NO ν A [8]

* These authors contributed equally to this work.
Corresponding author cvson@ifirse.icise.vn

Parameter	Best fit	3σ C.L. range
$\sin^2 \theta_{12}$	0.303	[0.270, 0.341]
$\sin^2 \theta_{13} (\times 10^{-2})$	2.203	[2.0, 2.4]
$\sin^2 \theta_{23}$	0.572	[0.406, 0.620]
$\delta_{CP} (^\circ)$	197	[108, 404]
$\Delta m_{21}^2 (10^{-5} \text{eV}^2/c^4)$	7.41	[6.82, 8.03]
$\Delta m_{31}^2 (10^{-3} \text{eV}^2/c^4)$	2.511	[2.428, 2.597]

TABLE I: Global constraints of neutrino oscillation parameters with *normal* mass ordering assumed, taken from Ref. [16] with NuFit 5.2 based on data available in November 2022.

and Super-Kamiokande (Super-K) [9] individually shows some mild preference to the *normal* mass ordering over the *inverted* one. Combining higher statistical samples from T2K and NO ν A with the reactor-based medium-baseline experiment JUNO [10] will be crucial for elucidating this unknown [11, 12]. One extra mystery in the PMNS 3-flavor picture is the parameterization-independent amplitude of CP violation, known as leptonic Jarlskog invariance, which is directly related to the CP-violation phase δ_{CP} as

$$J_{CP}^{\text{Lepton}} = \Im[U_{\alpha i} U_{\alpha j}^* U_{\beta i}^* U_{\beta j}] \quad (1)$$

$$= \frac{1}{8} \sin 2\theta_{12} \sin 2\theta_{23} \sin 2\theta_{13} \cos \theta_{13} \sin \delta_{CP}.$$

The T2K experiment [7, 13] has recently presented a significant hint on the non-zero CP-violation phase. However, NO ν A experiment [8] does not exhibit any similar inclination in the available data. The potential detection of the CP violation before the commencement of the next-generation accelerator-based neutrino experiments Hyper-Kamiokande (T2HK) [14] and DUNE [15] make the future joint analysis of T2K and NO ν A [11] a fascinating prospect. The final uncertainty pertains to the proximity of the mixing angle θ_{23} to $\pi/4$. As shown in Table I, the current 3σ C.L. range of $\sin^2 \theta_{23}$ encompasses around 21% of all possible values. The data strongly support the maximal mixing $\theta_{23} = \pi/4$ hypothesis. The near proximity of the mixing angle θ_{23} to maximal is an indication of a hidden symmetry between the second and third lepton generations, which are two distinct copies of the irreducible representations of $SU(2)_L$ group. The precise value of θ_{23} would be an important input to the flavor and neutrino mass models, as illustrated in Ref. [17, 18] and references therein.

This work aims to provide a concise overview of the uncertainty associated with measuring the θ_{23} mixing angle, estimate the possible reach of θ_{23} , and analyze its implications for a certain category of flavor models.

II. AMBIGUITY IN MEASURING THE θ_{23} MIXING ANGLE

The current knowledge of θ_{23} is mostly derived from neutrino oscillation measurements conducted using two sources: (i) atmospheric neutrinos and (ii) accelerator-based neutrinos. Joint analysis of accelerator-based and atmospheric neutrino sources in MINOS and MINOS+ experiments [19] results in $\sin^2 \theta_{23} = 0.43_{-0.04}^{+0.20}$. Measurement using the atmospheric neutrino data from Super-K [20] yields an interval of $0.41 \leq \sin^2 \theta_{23} \leq 0.58$ at the 90% C.L. Both current data from accelerator-based long-baseline T2K [7] and NO ν A [8] favor slightly the upper octant of the mixing angle θ_{23} . The current global fit data [16] using NuFit 5.2 supports the maximal mixing hypothesis at 90% C.L. The measurements from leading experiments and the global analysis of neutrino oscillation measurements are summarized in Table II. In long-baseline experiments using accelerator-based neutrino sources like ongoing T2K [24], and NO ν A [25], and forthcoming T2HK [14] and DUNE [15], the precise θ_{23} value can be extracted from measurements of $\nu_\mu (\bar{\nu}_\mu)$ -survival probabilities ($P(\nu_\mu \rightarrow \nu_\mu)$, $P(\bar{\nu}_\mu \rightarrow \bar{\nu}_\mu)$) or called as *disappearance* samples) and/or *appearances* of electron neutrinos from muon neutrinos ($P(\nu_\mu \rightarrow \nu_e)$, $P(\bar{\nu}_\mu \rightarrow \bar{\nu}_e)$) and known as *appearance* samples). Eq. (2) describes the survival probability of muon neutrinos around the oscillation maximum $\Phi_{31} \equiv 1.27 \times \Delta m_{31}^2 [\text{eV}^2] \frac{L[\text{km}]}{E[\text{GeV}]} \approx \pi/2$, which is applicable to T2K, NO ν A, and T2HK experimental setups.

$$P_{\nu_\mu \rightarrow \nu_\mu} (\Phi_{31} \approx \pi/2)$$

$$= 1 - (\cos^4 \theta_{13} \sin^2 2\theta_{23} + \sin^2 2\theta_{13} \sin^2 \theta_{23}) \sin^2 \Phi_{31}$$

$$+ \epsilon_m \Phi_{31} \sin 2\Phi_{31} (\cos^2 \theta_{12} \sin^2 2\theta_{23} - \sin^2 \theta_{23} J_{123} \cos \delta_{CP}), \quad (2)$$

where $\epsilon_m = \frac{\Delta m_{21}^2}{\Delta m_{31}^2}$ and $J_{123} = \sin 2\theta_{12} \sin 2\theta_{23} \sin 2\theta_{13}$. The leading order term of Eq. (2) reveals that the survival probability reaches its minimum at approximately $\sin^2 \theta_{23} \approx 0.5 \cos^{-2} \theta_{13} = 0.51$, given $\sin^2 \theta_{13} = 0.02203$. The survival oscillation probability $P_{\nu_\mu \rightarrow \nu_\mu}$ exhibits symmetry at this point and results in a discrete octant degeneracy: two discrete values of $\sin^2 \theta_{23}$ correspond to identical probabilities. To overcome the octant degeneracy in the *disappearance* channels, one approach is to utilize the sample of *appearance* data. Eq. (3) provides the approximate ν_e *appearance* probability around the oscillation maximum $\Phi_{31} \approx \pi/2$ in vacuum.

$$P_{\nu_\mu \rightarrow \nu_e} (\Phi_{31} \approx \pi/2) = \sin^2 \theta_{23} \sin^2 2\theta_{13} \sin^2 \Phi_{31}$$

$$+ \epsilon_m \Phi_{31} \sin \Phi_{31} J_{123} \cos(\Phi_{31} + \delta_{CP}), \quad (3)$$

The leading term of the ν_e *appearance* probability is determined by the factor $\sin^2 \theta_{23}$, making it highly responsive to the octant of θ_{23} . In addition, Eq. (3) shows that the magnitude of this flavor transition is modulated by both the poorly-established δ_{CP} and unknown neutrino

	T2K	NO ν A	MINOS	Super-K	IceCube	NuFIT 5.2
Best fit $\sin^2 \theta_{23}$	$0.561^{+0.019}_{-0.038}$	$0.57^{+0.03}_{-0.04}$	$0.43^{+0.20}_{-0.04}$	$0.425^{+0.051}_{-0.034}$	0.51 ± 0.05	$0.572^{+0.018}_{-0.023}$
Maximal rej. [σ]	1.22	1.29	0.90	1.25	0.28	1.69
Wrong-octant rej. [σ]	1.22	0.37	0.53	0.85	0	0.89
Constrained $\sin^2 \theta_{13}/10^{-2}$	2.18 ± 0.07	2.10 ± 0.11	2.10 ± 0.11	2.10 ± 0.11	2.224 ± 0.11	2.203 ± 0.0575

TABLE II: Current constraints on $\sin^2 \theta_{23}$ from T2K [7], NO ν A [21], MINOS(+) [19], Super-K [22], IceCube [23] and NUFIT 5.2 [16] with a *normal* mass ordering assumed.

mass ordering. Nevertheless, when both ν_e *appearance* and $\bar{\nu}_e$ *appearance* are measured with rather high statistical significance, the octant resolving has a marginal influence of the actual value of δ_{CP} . Besides, it is found that the relative difference in the probabilities of the ν_e ($\bar{\nu}_e$) *appearance* between the *normal* and *inverted* mass ordering is largely unaffected by the actual value of $\sin^2 \theta_{23}$ but only the true value of δ_{CP} . Consequently, the precise measurement of θ_{23} does not depend significantly on the neutrino mass ordering.

A relevant parameter which significantly influences the determination of the θ_{23} octant in case of non-maximal mixing is the precision value of θ_{13} . While the observation of $\nu_\mu \rightarrow \nu_e$ transition by T2K [26] established the non-zero value of θ_{13} , the most accurate measurement of this mixing angle is obtained from the reactor-based experiments [4]. From Eq. (3), the analytical formula to describe the continuous degeneracy between θ_{23} and θ_{13} can be formulated as

$$\sin 2\theta_{13}^{\text{true}} \sin \theta_{23}^{\text{true}} = \sin 2\theta_{13}^{\text{cloned}} \sin \theta_{23}^{\text{cloned}} \quad (4)$$

where $(\theta_{13}^{\text{true}}, \theta_{23}^{\text{true}})$ are true values and $(\theta_{13}^{\text{cloned}}, \theta_{23}^{\text{cloned}})$ are cloned solutions for a given $\nu_\mu \rightarrow \nu_e$ probability. This degeneracy suggests that the precision of the later will have a significant impact on the precision, as well as the octant resolving, of the former. Indeed, the effect has been observed in T2K data [7] where the data with and without reactor constraint on θ_{13} exhibits different preference for octant of θ_{23} . The reason is that T2K data itself favor a greater value of θ_{13} than the stringent constraint obtained from the reactor-based measurements. We provide a summary of the possible measurements in Fig. 1, which are displayed on the parameter space of θ_{23} - θ_{13} , in order to clarify the uncertainty in determining the mixing angle θ_{23} . For illustrative purpose, the true value of $\sin^2 \theta_{23}$ is set at 0.56 and $\sin^2 \theta_{13}$ is set at 0.02203. Using measurement with the $\nu_\mu \rightarrow \nu_\mu$ data channel, two distinct solutions will be obtained, one of which will be cloned in the lower octant. The curves of $\nu_\mu \rightarrow \nu_e$ and $\nu_e \rightarrow \nu_\tau$ iso-probabilities are orthogonal since the leading terms of the probabilities are proportional to $\sin^2 \theta_{23} \sin^2 2\theta_{13}$ for the former and $\cos^2 \theta_{23} \sin^2 2\theta_{13}$ for the later. Measurements made using $\nu_e \rightarrow \nu_e$ or $\bar{\nu}_e \rightarrow \bar{\nu}_e$ are marginally sensitive to θ_{23} but they are crucial for accurately measuring the θ_{13} value and hence valuable for resolving the octant of θ_{23} in case of non-maximal mixing. Recent measurements [16] have yielded a precision

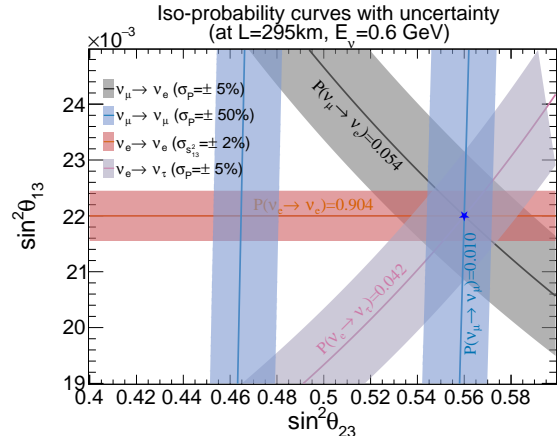


FIG. 1: Schematic view of addressing the ambiguity of θ_{23} is presented with the iso-probability curves in the $(\sin^2 \theta_{23}, \sin^2 \theta_{13})$ parameter space. The error band for each curve is obtained with a predefined uncertainty of probability σ_p . This includes $\nu_\mu \rightarrow \nu_\mu$, $\nu_\mu \rightarrow \nu_e$, $\nu_\mu \rightarrow \nu_\tau$, and $\nu_e \rightarrow \nu_e$ transitions. The true values of parameters are set to $\sin^2 \theta_{23} = 0.56$ and $\sin^2 \theta_{13} = 0.02203$ from NuFIT 5.2.

of 2.6% on $\sin^2 \theta_{13}$, corresponding to 1.3% uncertainty of θ_{13} . Furthermore, the value of $\sin^2 \theta_{13}$ can be improved to 1% (or 0.5% uncertainty of θ_{13}) [27]. The θ_{23} sensitivity will be calculated using these two constraints.

It is important to point out that the primary purpose of the θ_{23} measurements is to quantitatively assess the proximity of θ_{23} to the maximal mixing. This, as discussed in Sec. V, has considerable implications for testing the flavor models. From an empirical standpoint, this entails two consecutive hypothesis tests: (i) excluding the maximal mixing, and (ii) identifying the octant if non-maximal mixing is detected. The former can be quantitatively evaluated using statistics at a given θ_{23}^t in the vector of relevant parameter $\vec{\theta}$:

$$\Delta\chi_1^2(\vec{\theta}; \theta_{23}^t) = \chi_{\min.}^2(\vec{\theta}; \theta_{23} = \pi/4) - \chi_{\min.}^2(\vec{\theta}; \theta_{23}^{\text{b.f.}})$$

where $(\vec{\theta}; \theta_{23}^{\text{b.f.}})$ is the best-fit parameter vector, which ideally equals to $\vec{\theta}$ and $\theta_{23}^{\text{b.f.}} = \theta_{23}^t$. The statistical significance for the latter test is defined as the relative difference of χ^2 between the wrong-octant (W.O.) and the true-octant (T.O.) in the θ_{23} parameter space:

$$\Delta\chi_2^2(\vec{\theta}; \theta_{23}^t) = \chi_{\min.}^2(\vec{\theta}; \theta_{23}^{\text{b.f.}} \text{ in W.O.}) - \chi_{\min.}^2(\vec{\theta}; \theta_{23}^{\text{b.f.}} \text{ in T.O.})$$

Due to the continuity of the neutrino oscillation probability as function of θ_{23} , the statistical significance to exclude the maximal mixing is greater than that of excluding the wrong-octant. In the long-baseline accelerator-based experiments, the $\bar{\nu}_\mu \rightarrow \bar{\nu}_\mu$ *disappearance* samples are the more significant data sample for addressing the first hypothesis test, unless the actual $\sin^2 \theta_{23}$ exhibits a small deviation from the maximal mixing towards the higher octant. In contrast, the $\bar{\nu}_\mu \rightarrow \bar{\nu}_e$ *appearance* samples are crucial for resolving octants in case of non-maximal mixing.

III. EXPERIMENTAL SPECIFICATIONS OF T2HK, DUNE, ESSNU SB AND NEUTRINO FACTORY

In this section, we detail the experimental specifications for simulating the forthcoming accelerator-based long-baseline neutrino experiments T2HK and DUNE, along with proposed facilities ESSnuSB and Neutrino Factory.

T2HK and DUNE

Hyper-Kamiokande [14], a next-generation water Cherenkov detector that is approximately 8.4 times larger than its predecessor Super-Kamiokande, is a massive observatory under construction aimed at elucidating the mysteries of neutrinos, searching for proton decay, and investigating other new physics phenomena. This observatory is capable of detecting neutrinos from diverse natural (solar, atmospheric, astrophysical) and artificial (reactor, accelerator) sources. The Tokai to Hyper-Kamiokande (T2HK) program employs an intense and highly pure source of muon neutrinos and anti-neutrinos generated by the J-PARC accelerator, located 295 km away and at an angle of 2.5° from the average beam axis. This experimental setup is to achieve a narrow neutrino energy spectrum and enhance sensitivity to the relevant parameters, particularly CP-violation phase. The experiment is scheduled to commence data collection in 2027 and will continue for a duration of 10 years, equivalent to an exposure of 2.2×10^{22} protons-on-target (POT). This enables T2HK to collect approximately 10,000 $\nu_\mu(\bar{\nu}_\mu)$ events and 2,000 $\nu_e(\bar{\nu}_e)$ events, hence allowing T2HK to exclude CP conserving values ($\delta_{CP} = 0, \pm\pi$) at 5σ or greater C.L. for around 60% of δ_{CP} possible values. The neutrino mass ordering sensitivity of T2HK alone approaches 3σ C.L. However, a combined analysis with atmospheric neutrino data samples is anticipated to elevate the sensitivity to 5σ C.L. or greater within a specific range of neutrino oscillation parameters. Moreover, the T2HK allows to measure Δm_{32}^2 and $\sin^2 \theta_{23}$ parameters with remarkable precision, specifically 1% for the former and 0.6 - 1.7% for the later depending on its actual value. For simulation purpose, experimental specifications of T2HK

TABLE III: T2HK and DUNE main specifications for simulation, especially relevant to accelerator-based neutrino sources

Characteristics	T2HK [14]	DUNE [15]
Baseline	295 km	1284.9 km
Detector type	Water Cherenkov	Liquid Argon TPC
Detector mass	260 kton	40 kton
Beam power	1.3 MW	1.2 MW
Operation start ^a	2027	2031
Running time $\nu : \bar{\nu}$	2.5 yr : 7.5 yr	6.5 yr : 6.5 yr
ν energy range ^b	0.1 - 1.3 GeV	0.5 - 4.0 GeV
Systematic error ^c	signal: 3.2 - 3.9% background: 10%	signal: 2.0 - 5.0% background: 5-20%

^a based on status report at NuFACT2024 conference

^b relevant for oscillation measurements driven by Δm_{31}^2

^c the values depend on the selected samples

are based on the performance of its forerunner, T2K, as detailed in Ref. [11]. Tuning has been conducted to ensure compatibility with the proposed technical design report for T2HK [14], as illustrated in Appendix A.

Similar to Hyper-Kamiokande, the Deep Underground Neutrino Experiment (DUNE) [15] is a large-scale, multi-purpose neutrino experiment hosted by Fermilab, with its far detector located 1284.9 km away from the accelerator-based neutrino beam source. DUNE's far detector consists of four modular liquid argon time-projection chambers (TPC), totalling 40 kton. Over a planned thirteen-years operation (6.5 years for each neutrino and anti-neutrino modes), DUNE's far detector anticipates observing approximately 1000 $\nu_e(\bar{\nu}_e)$ and 10000 $\nu_\mu(\bar{\nu}_\mu)$ events [28]. This extensive statistics over such long experimental baseline enables DUNE to ascertain the neutrino mass ordering with significance of 5σ or above for all δ_{CP} actual values. In addition, DUNE can exclude CP conserving values of δ_{CP} at 5σ (3σ) or greater significance for 50% (75%) of the δ_{CP} true values. DUNE will improve the precision of other oscillation parameters, including $\sin^2 \theta_{23}, \sin^2 2\theta_{13}$. For the simulation of DUNE detector, we adopt the experimental configuration described in Ref. [15].

Main experimental specifications of T2HK and DUNE, especially for measurement of neutrino oscillation with the accelerator-based neutrino sources, are highlighted in Table III. The complementary between the two experiments for measuring oscillation parameters and testing leptonic mixing models has been investigated extensively [29, 30].

Proposed ESSnuSB and Neutrino Factory

The European Spallation Source Neutrino Super Beam (ESSnuSB) [31] proposes a long-baseline neutrino oscillation experiment that employs a 5 MW proton beam and

a 540 kton water Cherenkov detector. The objective is to accurately measure leptonic CP violation and explore potential new physics. The high precision of δ_{CP} , exceeding 8° for all potential values of δ_{CP} , enables ESSnuSB to evaluate certain categories of flavor models [32]. The experiment targets to measure neutrino oscillation at energies below 1 GeV, where charged-current quasi-elastic interactions predominate. A detector with 30% PMT optical coverage achieves a detection efficiency exceeding 85%, while maintaining a flavor mis-identification probability below 1%. Momentum resolution for (anti-)muons induced by $\nu_\mu(\bar{\nu}_\mu)$ charged-current interactions can range from 2.5% to 5.5%, while electron (positron) rings, produced by $\nu_e(\bar{\nu}_e)$, can range from 7.5% to 10.0%. In simulation, a normalization uncertainty of 5% is used for both signal and background in the selected samples. A total operational duration of approximately 10 years is assumed, divided equally between neutrino and antineutrino modes. Two candidates for the far detector site are evaluated, located at distances of 360 km and 540 km from the neutrino source. Our study, presented in Appendix B, shows that the experiment with former baseline achieves greater sensitivity to both $\cos \delta_{CP}$ and $\sin^2 \theta_{23}$, thereby providing enhanced utility for testing flavor models. Thus, unless otherwise specified, a baseline of 360 km is used for ESSnuSB in our study.

Neutrino Factory (NF) [33, 34] was proposed 25 years ago, around the discovery time of neutrino oscillation by Super-K, but before the discovery of relatively large θ_{13} . In this facility, the neutrino beam is produced through the decay-in-flight of high-energy (anti-)muons stored within a storage ring. The well-characterized neutrino flux, comprising two equally produced flavors (muon and electron) with opposite lepton numbers, facilitates the measurement of δ_{CP} and the determination of neutrino mass ordering across a broad range of θ_{13} values. A distinctive characteristic of a neutrino factory is its capability to measure neutrino oscillations at energies on the order of tens of GeV, enabling the study of transitions to tau neutrinos and facilitating tests of the unitarity of the PMNS matrix. A long baseline enables NF to examine non-standard physics scenarios across a broad parameter space with significant matter effects. The physical potentials of NF have been recently reexamined [35, 36], considering recent developments in the field and outlining potential directions following the T2HK and DUNE era. In NF's simulated configuration, operations over 8 years are equally divided between μ^- and μ^+ storage modes, with an assumed number of 1.06×10^{21} POT of 50 GeV muon decay-in-flight per year. A large detector with a fiducial mass of 50 kt, comparable to that of the Super-Kamiokande, is proposed to measure the $\nu_e(\bar{\nu}_e) \rightarrow \nu_\mu(\bar{\nu}_\mu)$ transitions with detection efficiencies of 45% (35%) and the $\nu_\mu(\bar{\nu}_\mu) \rightarrow \nu_e(\bar{\nu}_e)$ transitions with detection efficiencies of 90% (90%). A supplementary detector with a fiducial mass of 5 kt is proposed for the measurement of $\nu_e \rightarrow \nu_\tau$ oscillations, with a detection efficiency established at 9.6%. The energy resolution is

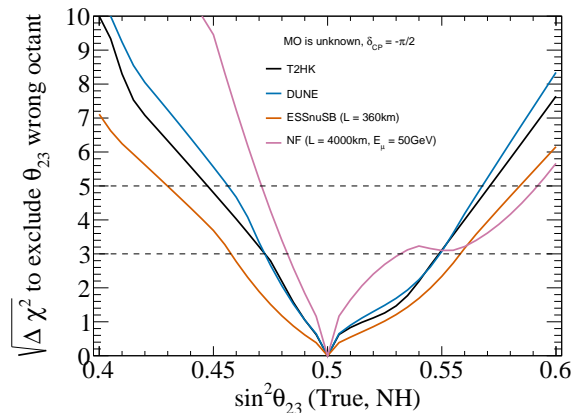


FIG. 2: The statistical significance to exclude the wrong-octant as function of $\sin^2 \theta_{23}$ with different experiments. Here $\delta_{CP} = -\pi/2$ is set, neutrino mass ordering (MO) is presumably unknown, and other relevant parameters and their uncertainties are taken from Table I.

established at $\sigma_E = 15\%$ for the former detector and 20% for the latter detector. For the purpose of cost-effectiveness analysis, it is assumed that these two detectors are positioned at the same baseline L . Two candidates for the experimental setup at the far detector site are proposed: 4000 km and 7500 km, corresponding to muon energies of 50 GeV and 30 GeV, respectively. Appendix B demonstrates that the baseline of 4000 km and $E_\mu = 50$ GeV, utilized primarily for this study unless otherwise noted, provides superior sensitivity for resolving the $\sin^2 \theta_{23}$ octant and achieving precision in $\cos \delta_{CP}$ compared to alternative configurations.

IV. PRECISION MEASUREMENT OF θ_{23} ANGLE

We utilize the GLoBES software [37, 38] to evaluate the sensitivity of neutrino experiments to the θ_{23} precision. The physics potential of neutrino experiments in addressing the octant of θ_{23} is characterized by which is so-called ‘‘octant blind region,’’ defined as the range of $\sin^2 \theta_{23}$ within which the actual octant cannot be established for a given statistical significance. The predicted octant-blind region of the future neutrino experiments are shown in Table IV. Both T2HK and DUNE experiments would be able to resolve the octant of mixing angle θ_{23} at 3σ C.L. if the true value of $\sin^2 \theta_{23}$ lies outside of the [0.47, 0.55] range. The proposed ESSnuSB is capable of accessing a slightly narrower region of θ_{23} . In neutrino factory, it is possible to investigate a wider range of mixing angle θ_{23} in both octants. The numbers presented in Table IV are calculated based on the existing limitations of the leptonic mixing parameters. An estimation using a 1% uncertainty on the

Exp.	Octant-blind regions of $\sin^2 \theta_{23}$	
	3 σ C.L.	5 σ C.L.
T2HK	[0.47, 0.55]	[0.45, 0.57]
DUNE	[0.47, 0.55]	[0.46, 0.57]
ESSnuSB	[0.46, 0.56]	[0.43, 0.58]
Nu-Factory	[0.48, 0.53]	[0.47, 0.59]

TABLE IV: The octant-blind regions at 3 σ and 5 σ C.L. of θ_{23} with individual T2HK and DUNE, ESSnuSB, and Neutrino Factory. Here the current constraint of θ_{13} is used.

Joint analysis	Octant-blind region of $\sin^2 \theta_{23}$	
	3 σ C.L.	5 σ C.L.
T2HK	[0.47, 0.55]	[0.45, 0.57]
+ DUNE	[0.48, 0.54]	[0.46, 0.56]
+ improved (θ_{13}, θ_{12})	[0.48, 0.54]	[0.47, 0.55]
+ ESSnuSB	[0.48, 0.53]	[0.47, 0.55]
+ Neutrino Factory	[0.49, 0.52]	[0.48, 0.53]

TABLE V: Octant-blind regions at 3 σ and 5 σ C.L. of θ_{23} with staging joint analyses

$\sin^2 \theta_{13}$ reveals that the 3 σ C.L. octant blind region can be narrowed down by less than 10%. More precisely, the percentage is around 8% for T2HK, 5% for DUNE and 9% for a combined analysis of T2HK and DUNE. While the precision of θ_{12} can achieve sub-percent accuracy with JUNO [39], its effect on the precision of θ_{23} is minimal. Nevertheless, this unprecedented θ_{12} constraint serves to narrow down the allowed range of parameters predicted by the flavor models outlined in Section V, allowing data to differentiate the models.

Our simulation, depicted in Fig. 3, suggests that T2HK and DUNE will conclusively establish the higher octant of θ_{23} for all values of θ_{23} within the currently fitted $\pm 1\sigma$ interval of parameter $\sin^2 \theta_{23} = 0.572_{-0.023}^{+0.018}$. However, if the actual value of $\sin^2 \theta_{23}$ falls within the range of [0.48, 0.54], its ambiguity can not be solved definitively with a statistical significance of 3 σ C.L. or higher, even with the use of T2HK, DUNE, or their joint analysis with envisaged constraints on θ_{13} and θ_{12} . In this scenario, possible solution to enhancing the reach of θ_{23} is to do a combined analysis of the T2HK and DUNE with the proposed ESSnuSB and Neutrino Factory. As shown in Fig. 3 and reported in Table. V, the octant ambiguity can be resolved at 3 σ C.L. if the truth value of $\sin^2 \theta_{23}$ lies outside of [0.49, 0.52]. This corresponds to a 50% reduction in the octant-blind region that remains inaccessible through a joint analysis of T2HK and DUNE. The interval [0.49, 0.52] is anticipated as the “dead” region for θ_{23} octant measurement.

V. IMPLICATIONS FOR THE LEPTONIC FLAVOR MODELS

That leptonic mixing, represented by two relatively large angles $\theta_{23} \approx \pi/4$, $\theta_{12} \approx \pi/6$, and one small angle $\theta_{13} \approx \pi/20$ in the PMNS matrix, is so different from the quark mixing, expressed by approximate unity CKM matrix, triggers questions whether the underlying symmetry is responsible for such patterns and how to describe them in a unified framework. Apparently, the question is relevant to unknown nature of neutrino mass. In this analysis, we examine a category of theoretical models in which the leptonic mixing matrix arises from the misalignment between the *flavor-definite* states $\{l_\alpha, \nu_\alpha\}$ and *symmetry* states $\{\tilde{l}_\alpha, \tilde{\nu}_\alpha\}$ of both charged and neutral leptons [17]. The weak charged-current is written as $J_\mu = \tilde{l}^\mu (1 - \gamma_5) \tilde{\nu} \equiv \tilde{l}^\mu (1 - \gamma_5) U_l^\dagger U_\nu \nu$ resulting in a formulation $U_{\text{PMNS}} = U_l^\dagger U_\nu$ where U_l and U_ν are unitary transformation matrices which rotate the states: $\tilde{l} = U_l l$ and $\tilde{\nu} = U_\nu \nu$; and diagonalize the mass matrices $U_l^\dagger M_l M_l^\dagger U_l = \text{diag}(m_e^2, m_\mu^2, m_\tau^2)$ and $U_\nu^T M_\nu U_\nu = \text{diag}(m_1, m_2, m_3)$. The mass matrices of charged and neutral leptons are assumed to be invariant when subjected to non-Abelian discrete symmetries G_l and G_ν respectively, which were commonly originated from a family symmetry G_f , see [40, 41] and references therein. Several $\{G_f \rightarrow G_l \oplus G_\nu\}$ models have been proposed to examine whether the hypothetical patterns of the leptonic mixing agrees with the measured neutrino parameters or not. Among them, the class of flavor models that involve the predictability of the less known δ_{CP} based on its relationship with other more precisely constrained mixing angles is of noteworthy interest because of its testability. The so-called *solar* sum rules [42], in which U_ν is characterized by a maximal $\theta_{23}^\nu = \pi/4$ rotation in 2-3 generation plane, a predetermined θ_{12}^ν in 1-2 generation plane, and non-diagonal U_l to account for relatively smallness of the θ_{13} angle, establish following relation:

$$\cos \delta_{\text{CP}} = \frac{\tan \theta_{23}}{\sin 2\theta_{12} \sin \theta_{13}} [\cos 2\theta_{12}^\nu + (\sin^2 \theta_{12} - \cos^2 \theta_{12}^\nu)(1 - \cot^2 \theta_{23} \sin^2 \theta_{13})]. \quad (5)$$

The values of $\sin \theta_{12}^\nu$ are fixed at (i) $1/\sqrt{2}$, (ii) $1/\sqrt{3}$, (iii) $1/2$, (iv) $1/\sqrt{\sqrt{5}r_g}$, (v) $\sqrt{3-r_g}/2$, (vi) $\sqrt{(2-r_g)/3}$ where golden ratio $r_g = (1 + \sqrt{5})/2$, depending on the symmetry form of the U_ν matrices, which are, respectively, (i) bi-maximal (BM), (ii) tri-bimaximal (TBM), (iii) hexagonal (HG), (iv) golden rule type A (GRA), (v) golden rule type B (GRB), and (vi) golden rule type C (GRC). Eq. (5) exhibits a non-negligible dependence of δ_{CP} on the θ_{23} , particularly deviation of $\cos \delta_{\text{CP}}$ from zero is greater as the value of θ_{23} increases. It is observed that the BM and GRC models are disfavored since a valid δ_{CP} acquires θ_{23} to be out of the current 3 σ C.L. allowed range of this parameter. The remaining four models pre-

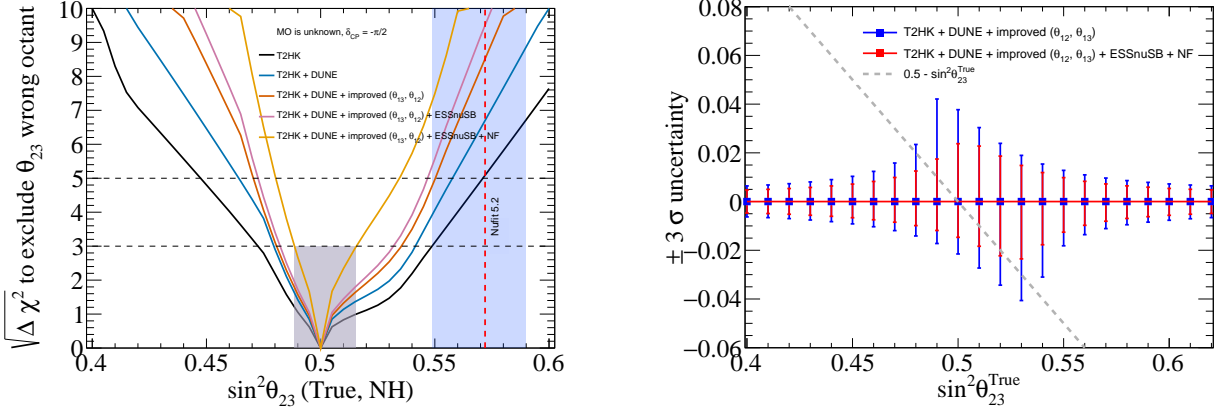


FIG. 3: The left plot presents statistical significance to exclude the wrong-octant as a function of $\sin^2 \theta_{23}$ with T2HK and various configurations of joint analyses. The right plot is the $\pm 3\sigma$ uncertainty as function of true values of $\sin^2 \theta_{23}$ with joint analyses. Here $\delta_{CP} = -\pi/2$ is set, MO is presumably unknown.

dict significant amount of the CP violation. Alternative models, in which U_l is assumed to be diagonal and symmetry pattern of U_ν to be partially broken to formulate empirically the observed PMNS matrix, have also been investigated [43]. There are two *atmospheric* sum rules, known as TM1 and TM2, depending on the first or second column of the tri-bimaximal form of U_ν kept to be conserved. TM1 and TM2 establish a relation between θ_{12} and θ_{13} mixing angles, specified as $\sin^2 \theta_{12} = \frac{1-3\sin^2 \theta_{13}}{3(1-\sin^2 \theta_{13})}$ and $\sin^2 \theta_{12} = \frac{1}{3(1-\sin^2 \theta_{13})}$ respectively. The predictions are consistent in 3σ C.L. with the current constraint of oscillation parameters shown in Table I. These predictions will be further tested by future neutrino experiments, when the precision of both θ_{12} and θ_{13} mixing angle will be improved. Moreover, TM1 and TM2 enforce a relationship between δ_{CP} and other mixing parameters [43], provided in Eq. (6).

$$\cos \delta_{CP} = \begin{cases} -\frac{(1-5\sin^2 \theta_{13}) \cot 2\theta_{23}}{2\sqrt{2} \sin \theta_{13} \sqrt{1-3\sin^2 \theta_{13}}} & \text{(TM1)} \\ \frac{(1-2\sin^2 \theta_{13}) \cot 2\theta_{23}}{\sin \theta_{13} \sqrt{2-3\sin^2 \theta_{13}}} & \text{(TM2)} \end{cases} \quad (6)$$

In comparison to the *solar* sum rules, the *atmospheric* sum rules exhibit a more profound correlation between the value of δ_{CP} and the value of θ_{23} . The allowed parameter space of $(\delta_{CP}, \theta_{23})$ of the above-mentioned flavor models are presented in Fig. 4. Given the current 3σ C.L. range of $\sin^2 \theta_{23}$, all models, with the exception of the BM and GRC which are not consistent with data, predict a substantial violation of the CP symmetry in the lepton sector. The difference between *solar* sum rules are relatively small due to the uncertainties on θ_{12} and θ_{13} . Fig. 5 shows the allowed parameter space in $(\delta_{CP}, \theta_{23})$ of the flavor models, assuming that the central values of $\sin^2 \theta_{12}$ and $\sin^2 \theta_{13}$ remain unchanged, but their uncertainty is decreased to 0.5% and 1.0% respectively. In comparison to Fig. 4, the predicted parameter space from different *solar* sum rules become more distinguish-

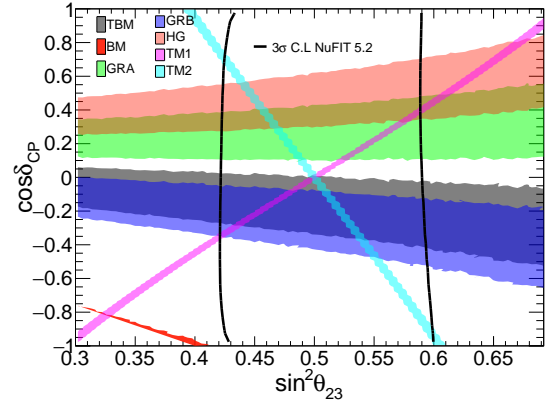


FIG. 4: Allowed parameter spaces of $(\delta_{CP}, \theta_{23})$ with flavor models are overlaid with current constraint of the global neutrino data.

able, thereby enhancing the test capability. We find that if CP is conserved, a joint analysis of T2HK and DUNE would be sensitive enough to eliminate all *solar* and *atmospheric* TM1 sum rules for all possible allowed value of θ_{23} . The CP conservation is still applicable for TM2 if θ_{23} is significantly deviated from the maximal mixing, specifically when actual value of $\sin^2 \theta_{23}$ is close to 0.4 in lower octant or 0.6 in higher octant. Thus the measurement of θ_{23} (in addition to θ_{12}) measurement will settle the test for TM2. For maximum CP violation ($\cos \delta_{CP} = 0$), we find that uncertainty of $\cos \delta_{CP}$ of the combination between T2HK and DUNE, which is around the range of $[-0.4, 0.5]$ at 3σ C.L., is not sufficient for differentiating the *solar* and *atmospheric* TM1 sum rule. If actual $\sin^2 \theta_{23}$ falls outside of $[0.44, 0.56]$, the analysis of T2HK and DUNE will rule out the *atmospheric* TM2 sum rule. Fig. 5 includes a possibility of $\cos \delta_{CP} - \sin^2 \theta_{23}$ sensi-

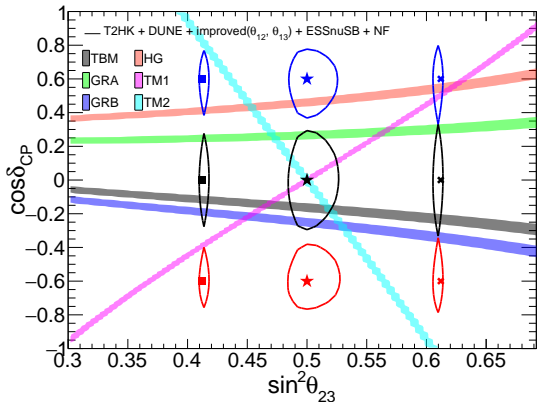


FIG. 5: The allowed parameter space of $(\delta_{CP}, \theta_{23})$ with flavor models is tightened when applying more precise measurements of θ_{13}, θ_{12} . The sensitivity contours of future constraints at some actual values of parameters are computed with joint analysis of simulated data using T2HK, DUNE, ESSnuSB and Neutrino Factory.

tivity using a combined T2HK, DUNE, ESSnuSB and Neutrino Factory. It is found that this ultimate analysis, which can achieve precision of $\cos \delta_{CP}$ around the range of $[-0.25, 0.30]$, will rule out the *solar* HG sum rule in entire parameter space of θ_{23} . Also, the enhancement in the $\cos \delta_{CP}$ precision also helps to eliminate the *atmospheric* TM1 and TM2 models if $\sin^2 \theta_{23}$ is found to out of the range of $[0.44, 0.57]$ and $[0.47, 0.53]$ respectively. However, the sensitivity of this ultimate reach on $\cos \delta_{CP}$ is not sufficient to distinguish the *solar* TBM, GRA, GRB sum rules.

VI. SUMMARY

The present landscape of the neutrino oscillation measurement indicates that θ_{23} is in close proximity to the maximal mixing. We explore the optimum extent of this mixing angle by analysis of forthcoming influential experiments, T2HK and DUNE with potential future in-

clusion of ESSnuSB and the neutrino factory. Our findings indicate that the accuracy of this measurement does not depend significantly on the truth value as well as the precision of δ_{CP} . Furthermore, it is not affected by the unidentified neutrino mass ordering. As long as the actual value falls within the current $\pm 1\sigma$ interval, both T2HK and DUNE can assert the higher octant of θ_{23} . However, if the value of θ_{23} is within the octant-blind region of $[0.48, 0.54]$ at 3σ C.L., these experiments cannot resolve the ambiguity of this parameter. A possible solution is to have a joint analysis of T2HK and DUNE with ESSnuSB and Neutrino Factory, provided that the data is available. Within this scenario, the octant-blind region will be narrowed down to a range of $[0.49, 0.52]$. The precision measurement of θ_{23} , together with the δ_{CP} precision, are essential for testing a category of flavor models that result in an exact relationship between these two parameters via the *solar* and *atmospheric* sum rules. We find that if CP is conserved, the combined sensitivity between T2HK and DUNE will eliminate nearly all of these models. In the case that the CP is maximally violated, only *atmospheric* TM2 can be excluded if real value of θ_{23} is significantly deviated from $\pi/4$. Conducting a combined analysis of the two aforementioned experiments with ESSnuSB and Neutrino factory, if available, can effectively eliminate the *solar* HG sum rules and both *atmospheric* TM1 and TM2 sum rules in certain range of θ_{23} . Nevertheless, the overall sensitivity is inadequate to tell preference of data to particular *solar* sum rule model among TBM, GRA, and GRB models.

ACKNOWLEDGEMENT

S. Cao would like to thank KEK for their hospitality during his visit. A. Nath wishes to express gratitude to IFIRSE, ICISE for their hospitality. Phan To Quyen was funded by the Master, PhD Scholarship Programme of Vingroup Innovation Foundation (VINIF), code VINIF.2023.TS.095. The research of S. Cao and N. T. H. Van is funded by the National Foundation for Science and Technology Development (NAFOSTED) of Vietnam under Grant No. 103.99-2023.144.

-
- [1] Y. Fukuda *et al.* (Super-Kamiokande Collaboration), “Evidence for oscillation of atmospheric neutrinos,” *Phys. Rev. Lett.* **81**, 1562 (1998), arXiv:hep-ex/9807003.
- [2] Q. Ahmad *et al.* (SNO Collaboration), “Measurement of the rate of $\nu_e + d \rightarrow p + p + e^-$ interactions produced by 8B solar neutrinos at the Sudbury Neutrino Observatory,” *Phys. Rev. Lett.* **87**, 071301 (2001), arXiv:0106015 [nucl-ex].
- [3] Q. R. Ahmad *et al.* (SNO), “Measurement of day and night neutrino energy spectra at SNO and constraints on neutrino mixing parameters,” *Phys. Rev. Lett.* **89**, 011302 (2002), arXiv:nucl-ex/0204009.
- [4] S. Navas *et al.* (Particle Data Group), “Review of particle physics,” *Phys. Rev. D* **110**, 030001 (2024).
- [5] B. Pontecorvo, “Neutrino experiments and the problem of conservation of leptonic charge,” *Sov. Phys. JETP* **26**, 165 (1968).
- [6] Z. Maki, M. Nakagawa, and S. Sakata, “Remarks on the unified model of elementary particles,” *Prog. Theor. Phys.* **28**, 870 (1962).
- [7] K. Abe *et al.* (T2K), “Measurements of neutrino oscillation parameters from the T2K experiment using 3.6×10^{21} protons on target,” *Eur. Phys. J. C* **83**, 782 (2023), arXiv:2303.03222 [hep-ex].

- [8] M. Acero, P. Adamson, L. Aliaga, N. Anfimov, A. Antoshkin, E. Arrieta-Diaz, L. Asquith, A. Aurisano, A. Back, C. Backhouse, *et al.*, “Improved measurement of neutrino oscillation parameters by the *no ν A* experiment,” *Physical Review D* **106**, 032004 (2022).
- [9] T. Wester *et al.* (Super-Kamiokande), “Atmospheric neutrino oscillation analysis with neutron tagging and an expanded fiducial volume in Super-Kamiokande I–V,” *Phys. Rev. D* **109**, 072014 (2024), arXiv:2311.05105 [hep-ex].
- [10] Z. Djurcic *et al.* (JUNO Collaboration), “JUNO Conceptual Design Report,” (2015), arXiv:1508.07166 [physics.ins-det].
- [11] S. Cao, A. Nath, T. V. Ngoc, P. T. Quyen, N. T. Hong Van, and N. K. Francis, “Physics potential of the combined sensitivity of T2K-II, NO ν A extension, and JUNO,” *Phys. Rev. D* **103**, 112010 (2021), arXiv:2009.08585 [hep-ph].
- [12] A. Cabrera *et al.*, “Synergies and prospects for early resolution of the neutrino mass ordering,” *Sci. Rep.* **12**, 5393 (2022), arXiv:2008.11280 [hep-ph].
- [13] K. Abe *et al.* (T2K), “Constraint on the matter–antimatter symmetry-violating phase in neutrino oscillations,” *Nature* **580**, 339 (2020), [Erratum: *Nature* **583**, E16 (2020)], arXiv:1910.03887 [hep-ex].
- [14] K. A. Hyper-Kamiokande Proto-Collaboration, *et al.*, “Hyper-kamiokande design report,” (2018), arXiv:1805.04163 [physics.ins-det].
- [15] B. Abi *et al.* (DUNE), “Experiment Simulation Configurations Approximating DUNE TDR,” (2021), arXiv:2103.04797 [hep-ex].
- [16] I. Esteban, M. C. Gonzalez-Garcia, M. Maltoni, T. Schwetz, and A. Zhou, “The fate of hints: updated global analysis of three-flavor neutrino oscillations,” *JHEP* **09**, 178 (2020), arXiv:2007.14792 [hep-ph].
- [17] R. N. Mohapatra and A. Y. Smirnov, “Neutrino Mass and New Physics,” *Ann. Rev. Nucl. Part. Sci.* **56**, 569 (2006), arXiv:hep-ph/0603118.
- [18] J. Gehrlein, S. Petcov, M. Spinrath, and A. Titov, “Testing neutrino flavor models,” in *Snowmass 2021* (2022) arXiv:2203.06219 [hep-ph].
- [19] P. Adamson *et al.* (MINOS+), “Precision Constraints for Three-Flavor Neutrino Oscillations from the Full MINOS+ and MINOS Dataset,” *Phys. Rev. Lett.* **125**, 131802 (2020), arXiv:2006.15208 [hep-ex].
- [20] R. Wendell *et al.* (Super-Kamiokande), “Atmospheric neutrino oscillation analysis with sub-leading effects in Super-Kamiokande I, II, and III,” *Phys. Rev. D* **81**, 092004 (2010), arXiv:1002.3471 [hep-ex].
- [21] M. A. Acero *et al.* (NO ν A), “Improved measurement of neutrino oscillation parameters by the NO ν A experiment,” *Phys. Rev. D* **106**, 032004 (2022), arXiv:2108.08219 [hep-ex].
- [22] M. Jiang *et al.* (Super-Kamiokande), “Atmospheric Neutrino Oscillation Analysis with Improved Event Reconstruction in Super-Kamiokande IV,” *PTEP* **2019**, 053F01 (2019), arXiv:1901.03230 [hep-ex].
- [23] R. Abbasi *et al.* ((IceCube Collaboration)*, IceCube), “Measurement of atmospheric neutrino mixing with improved IceCube DeepCore calibration and data processing,” *Phys. Rev. D* **108**, 012014 (2023), arXiv:2304.12236 [hep-ex].
- [24] K. Abe *et al.* (T2K Collaboration), “The T2K experiment,” *Nucl. Instrum. Methods Phys. Res. Sect. A* **659**, 106 (2011), arXiv:1106.1238 [physics.ins-det].
- [25] D. Ayres *et al.* (NO ν A Collaboration), “The NO ν A Technical Design Report,” (2007), 10.2172/935497.
- [26] K. Abe *et al.* (T2K), “Observation of Electron Neutrino Appearance in a Muon Neutrino Beam,” *Phys. Rev. Lett.* **112**, 061802 (2014), arXiv:1311.4750 [hep-ex].
- [27] J. Zhang and J. Cao, “Towards a sub-percent precision measurement of $\sin^2\theta_{13}$ with reactor antineutrinos,” *JHEP* **03**, 072 (2023), arXiv:2206.15317 [hep-ex].
- [28] J. Strait *et al.* (DUNE), “Long-Baseline Neutrino Facility (LBNF) and Deep Underground Neutrino Experiment (DUNE): Conceptual Design Report, Volume 3: Long-Baseline Neutrino Facility for DUNE June 24, 2015,” (2016), arXiv:1601.05823 [physics.ins-det].
- [29] S. Fukasawa, M. Ghosh, and O. Yasuda, “Complementarity Between Hyperkamiokande and DUNE in Determining Neutrino Oscillation Parameters,” *Nucl. Phys. B* **918**, 337 (2017), arXiv:1607.03758 [hep-ph].
- [30] S. K. Agarwalla, S. S. Chatterjee, S. T. Petcov, and A. V. Titov, “Addressing Neutrino Mixing Models with DUNE and T2HK,” *Eur. Phys. J. C* **78**, 286 (2018), arXiv:1711.02107 [hep-ph].
- [31] S. Rosauero Alcaraz, M. Blennow, E. Fernandez-Martinez, and T. Ota, “Physics potential of the ESSnuSB,” *PoS NuFact2021*, 063 (2022).
- [32] M. Blennow, M. Ghosh, T. Ohlsson, and A. Titov, “Testing Lepton Flavor Models at ESSnuSB,” *JHEP* **07**, 014 (2020), arXiv:2004.00017 [hep-ph].
- [33] S. Geer, “Neutrino beams from muon storage rings: Characteristics and physics potential,” *Phys. Rev. D* **57**, 6989 (1998), [Erratum: *Phys.Rev.D* **59**, 039903 (1999)], arXiv:hep-ph/9712290.
- [34] S. Choubey *et al.* (IDS-NF), “International Design Study for the Neutrino Factory, Interim Design Report,” (2011), arXiv:1112.2853 [hep-ex].
- [35] A. Bogacz *et al.*, “The Physics Case for a Neutrino Factory,” in *Snowmass 2021* (2022) arXiv:2203.08094 [hep-ph].
- [36] P. B. Denton and J. Gehrlein, “A Modern Look at the Oscillation Physics Case for a Neutrino Factory,” (2024), arXiv:2407.02572 [hep-ph].
- [37] P. Huber, M. Lindner, and W. Winter, “Simulation of long-baseline neutrino oscillation experiments with GLOBES (General Long Baseline Experiment Simulator),” *Comput. Phys. Commun.* **167**, 195 (2005), arXiv:hep-ph/0407333.
- [38] P. Huber, J. Kopp, M. Lindner, M. Rolinec, and W. Winter, “New features in the simulation of neutrino oscillation experiments with GLOBES 3.0: General Long Baseline Experiment Simulator,” *Comput. Phys. Commun.* **177**, 432 (2007), arXiv:hep-ph/0701187.
- [39] A. Abusleme *et al.* (JUNO), “Sub-percent precision measurement of neutrino oscillation parameters with JUNO,” *Chin. Phys. C* **46**, 123001 (2022), arXiv:2204.13249 [hep-ex].
- [40] G. Altarelli and F. Feruglio, “Discrete Flavor Symmetries and Models of Neutrino Mixing,” *Rev. Mod. Phys.* **82**, 2701 (2010), arXiv:1002.0211 [hep-ph].
- [41] S. F. King and C. Luhn, “Neutrino Mass and Mixing with Discrete Symmetry,” *Rept. Prog. Phys.* **76**, 056201 (2013), arXiv:1301.1340 [hep-ph].
- [42] S. T. Petcov, “Predicting the values of the leptonic CP violation phases in theories with discrete flavour symmetries,” *Nucl. Phys. B* **892**, 400 (2015), arXiv:1405.6006

[hep-ph].

- [43] F. Costa and S. F. King, “Neutrino Mixing Sum Rules and the Littlest Seesaw,” *Universe* **9**, 472 (2023), arXiv:2307.13895 [hep-ph].

Appendix A: Simulated event rates of T2HK

The simulated experimental configuration of T2HK, as outlined in the technical design report (TDR) [14], is presented in Table VI, along with basic features listed in Table III. The event rate of four simulated data samples for neutrino oscillation measurements, closely aligned with the T2HK TDR, is presented in Fig. 6. This study employs a tuning of detection efficiency as a function of energy to match with the TDR report, enabling us to closely approach the physical potential of T2HK in measuring neutrino oscillation parameters.

Appendix B: Optimization of ESSnuSB and Neutrino Factory

Both ESSnuSB and Neutrino Factory exhibit some flexibility in their current designs. Our selection is grounded in the optimal sensitivity achieved concurrently on both δ_{CP} , specifically the precision of $\cos\delta_{CP}$ and $\sin^2\theta_{23}$, which are crucial for evaluating the class of flavor models discussed in Section V. We examine the physical sensitivity of these parameters in the context of ESSnuSB, utilizing two different detector baseline options. The left plot of Fig. 7 demonstrates that a baseline of 360 km yields superior performance compared to a baseline of 540 km. This study examines two scenarios for the Neutrino Factory: one with a muon energy of 50 GeV and a baseline of 4000 km, and another with a muon energy of 30 GeV and the same baseline of 4000 km. The left plot of Fig. 7 clearly indicates that the former scenario is anticipated to provide improved sensitivity to both $\cos\delta_{CP}$ and $\sin^2\theta_{23}$. Furthermore, it has been observed that ESSnuSB significantly enhances the precision of $\cos\delta_{CP}$, whereas the Neutrino Factory provides superior sensitivity regarding the octant of θ_{23} . The inclusion of both ESSnuSB and Neutrino Factory is complementary for the precise measurement of both $\cos\delta_{CP}$ and $\sin^2\theta_{23}$, thereby enhancing our sensitivity to test the class of flavor models discussed in Section V.

TABLE VI: T2HK specifications for simulation, based on Ref [14], along with Table III

Characteristics	T2HK experimental setup for simulation [14]
Matter density	2.6 gcc^{-1}
Signal and background efficiency	
-Appearance	
ν mode ($\nu_\mu \rightarrow \nu_e$)	61.6% ν_e QE, 48.5% $\bar{\nu}_e$ QE 0.076% ν_μ CC, 23.6% ν_e beam and 12.1% $\bar{\nu}_e$ beam, 0.31% ν_μ NC
$\bar{\nu}$ mode ($\bar{\nu}_\mu \rightarrow \bar{\nu}_e$)	68.6% $\bar{\nu}_e$ QE, 43.6% ν_e QE 0.023% ν_μ CC, 0.015% $\bar{\nu}_\mu$ CC, 13% ν_e beam and 29.6% $\bar{\nu}_e$ beam, 0.9% $\bar{\nu}_\mu$ NC
-Disappearance	
ν mode ($\nu_\mu \rightarrow \nu_\mu$)	(69.7%, 15.7%) ^a ν_μ , (73.2%, 40.6%) $\bar{\nu}_\mu$ 1.01% ν_e CC, 0.42% ν_e beam and 0.6% $\bar{\nu}_e$ beam, 1.1% ν_μ NC
$\bar{\nu}$ mode ($\bar{\nu}_\mu \rightarrow \bar{\nu}_\mu$)	(73.1%, 41.5%) $\bar{\nu}_\mu$, (67.4%, 15.2%) ν_μ 0.46% ν_e CC, 0.09% ν_e beam and 0.3% $\bar{\nu}_e$ beam, 2.79% $\bar{\nu}_\mu$ NC
Systematics	
-Signal ^b	3.2% (2.5%) ν_e appearance, 3.9% (2.5%) $\bar{\nu}_e$ appearance 3.6% (2.5%) ν_μ disappearance, 3.6% (2.5%) $\bar{\nu}_\mu$ disappearance
-Background ^c	10% (2.5%)
Energy resolution	$0.03/\sqrt{E(\text{GeV})}$
Energy window	0.10 : 1.30 GeV (APP), 0.20 : 5.05 GeV (DIS)

^a (CCQE, CC-nonQE) where CC : Charged-Current and QE : Quasi-Elastic scattering

^b normalization (calibration) error for signal

^c normalization (calibration) error for background

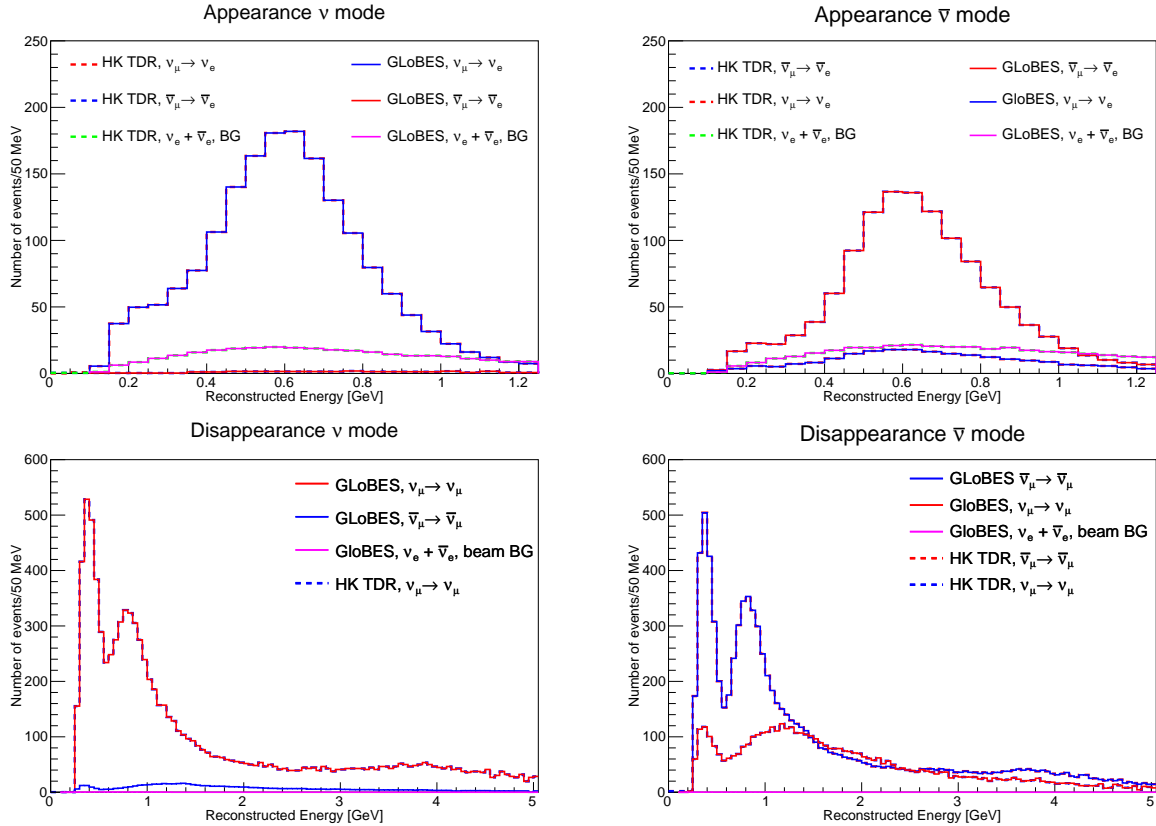


FIG. 6: The event spectra for the signal and background in the T2HK simulated sample are presented as a function of reconstructed neutrino energy. The upper (lower) spectrum corresponds to the *appearance* (*disappearance*) channel, while the left (right) spectrum involves to the ν -mode ($\bar{\nu}$ -mode) respectively. *Normal* mass ordering (MO), $\delta_{CP} = 0$, and other oscillation parameters provided in the Technical Design Report (TDR) [14] are assumed for the rate calculation.

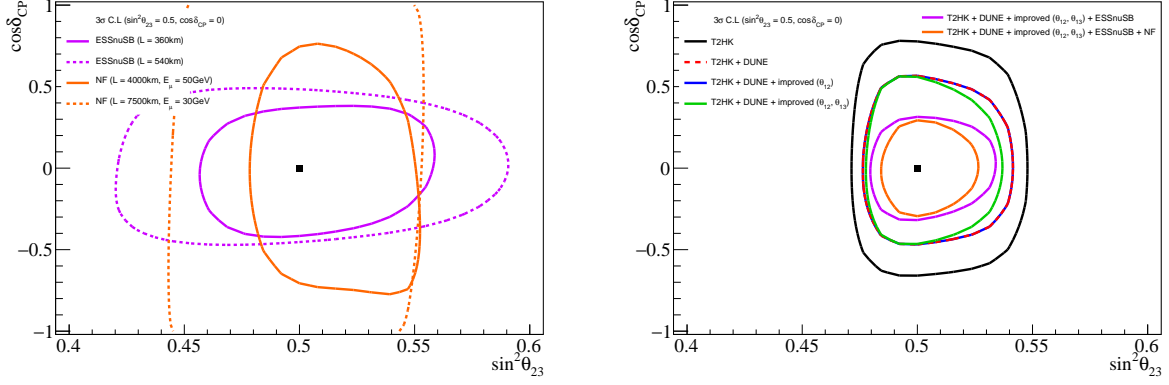


FIG. 7: Left shows comparison of allowed parameter space in $(\cos \delta_{CP}, \sin^2 \theta_{23})$ using ESSnuSB and NF with different baseline options. The sensitivity of joint analyses involving T2HK and DUNE to $\delta_{CP} - \theta_{23}$ measurements is illustrated on the right, utilizing ESSnuSB with baseline of 360km and NF with 4000 km baseline and 50 GeV of stored muons. Study is done at $\cos \delta_{CP} = 0$ and $\sin^2 \theta_{23} = 0.5$, while the other parameters are constrained by the global fit data.